Eur. Phys. J. B **59**, 343–356 (2007)
DOI: 10.1140/epjb/e2007-00288-x

THE EUROPEAN PHYSICAL JOURNAL B

Density and stability in ultracold dilute boson-fermion mixtures

S. Röthel[1,a] and A. Pelster[2,b]

[1] Westfälische Wilhelms-Universität Münster, Wilhelm-Klemm-Straße 9, 48149 Münster, Germany
[2] Universität Duisburg-Essen, Campus Duisburg, Fachbereich Physik, Lotharstraße 1, 47048 Duisburg, Germany

Received 11 May 2007 / Received in final form 20 August 2007
Published online 17 October 2007 –

Abstract. We analyze in detail recent experiments on ultracold dilute ^{87}Rb–^{40}K mixtures in Hamburg and in Florence within a mean-field theory. To this end we determine how the stationary bosonic and fermionic density profiles in this mixture depend in the Thomas-Fermi limit on the respective particle numbers. Furthermore, we investigate how the observed stability of the Bose-Fermi mixture with respect to collapse is crucially related to the value of the interspecies s-wave scattering length.

PACS. 03.75.Hh Static properties of condensates; thermodynamical, statistical, and structural properties

1 Introduction

Six years after the first experimental achievement of Bose-Einstein condensation (BEC) of trapped atomic gases in 1995 fermionic atomic gases were brought together with bosonic atoms to quantum degeneracy in a ^{7}Li–^{6}Li mixture [1,2], ^{23}Na–^{6}Li mixture [3], and ^{87}Rb–^{40}K mixture [4]. In contrast to a pure Bose system, quantum degeneracy in a Fermi system with only one spin component means for $T \ll T_F = E_F/k_B$ that all energy states below the Fermi energy E_F are occupied with one fermion each, whereas all states above E_F remain empty. The main problem to achieve quantum degeneracy in a Fermi gas is the inability of fermions to be directly evaporatively cooled. Due to the Pauli exclusion principle, fermions in the same spin polarized hyperfine state are not allowed to be close together, so that they can not collide via short-range contact interaction to rethermalize the gas during the evaporative cooling. This handicap was circumvented in the experiment of reference [5], where a mixture with two different spin states of ^{40}K was simultaneously evaporated by mutual cooling. In combination with a Bose gas the fermions are sympathetically cooled by elastic interactions with the bosons in the overlapping region [4,6].

Beside the exploration of quantum degeneracy, one is also interested in studying how the two-particle interaction influences the system properties. Mixtures with a strong interspecies interaction, with the prominent example of ^{4}He–^{3}He liquid [7,8], lead to new phenomena like phase separation or BEC-induced interactions between fermions. Depending on the nature of the interspecies interaction, a repulsion between bosons and fermions tends to a demixing in order to minimize the overlapping region [9], whereas in the case of an attraction the mixture can collapse as long as the particle numbers are sufficiently large [6,10]. The possibility of superfluidity in a Fermi gas, especially the predicted BEC-BCS crossover between BCS-type superfluidity of Cooper pairs of fermionic atoms and BEC of molecules was recently probed [11,12]. A Feshbach resonance was used to tune the interaction strength between fermionic atoms of two different spin states, characterized by the s-wave scattering length a, from effectively repulsive ($a > 0$) to attractive ($a < 0$). On the BEC side ($a > 0$) of the magnetic field resonance, there exists a weakly bound molecular state. Fermionic atoms are bound into bosonic molecules which can condense at sufficient low temperatures. On the BCS side ($a < 0$) of the resonance two fermions with different spin states form a loosely bounded Cooper pair. The condensation of fermionic atom pairs was observed on both the BEC and the BCS side of the Feshbach resonance in the experiment [11,12]. Furthermore, the system properties were observed to vary smoothly in the BEC-BCS crossover regime. An alternative and complementary access to Fermi superfluidity is expected from quantum degenerate Bose-Fermi mixtures where an effective interaction between fermions is mediated by the bosons [13,14], similarly to phonons in a solid-state superconductor.

Another recent and fast growing field is the investigation of ultracold boson-fermion mixtures trapped in an optical lattice which is created by standing waves of the electric field of counterpropagating laser beams. The atoms can be confined to different lattice sites and, by varying the laser intensity, their tunneling to neighboring sites as well as the strength of their on-site repulsive interactions can be controlled. In the case of a pure ultracold Bose-Einstein condensate with repulsive interaction, held

[a] e-mail: steffen.roethel@uni-muenster.de
[b] e-mail: axel.pelster@uni-duisburg-essen.de

in a three-dimensional optical lattice potential, a quantum phase transition from a superfluid to a Mott insulator phase was observed as the depth of the lattice is increased leading to a suppression of the tunneling between neighboring lattice sites [15]. The presence of fermionic atoms together with the Bose-Einstein condensate makes the system more complex and richer in its behavior at low temperatures. It has been predicted that novel quantum phases in the strong-coupling regime occur which involve the pairing of fermions with one or more bosons or bosonic holes, respectively, when the boson-fermion interaction is attractive or repulsive [16]. Depending on the physical parameters of the system, these composite fermions may appear as a normal Fermi liquid, a density wave, a superfluid, or an insulator with fermionic domains. Instead of varying the lattice potential depth the transition from a superfluid to a Mott insulator in bosonic ^{87}Rb can be shifted towards larger lattice depth by adding fermionic ^{40}K which interacts attractively with rubidium and therefore increases the effective lattice depth [17,18].

Ultracold trapped boson-fermion mixtures were investigated with respect to a demixing of the components [19–21] and to a collapse due to the interspecies attraction [20–24]. Furthermore, the time-dependent dynamics of the collapse [25] and finite temperature effects on the stability in a boson-fermion mixture were also studied [26]. Our theoretical investigation is based on the experiments with a ^{87}Rb–^{40}K boson-fermion mixture in a harmonic trap, which were performed in Hamburg [6] and in Florence [4,10]. After cooling down at a temperature below 1 μK, a condensate of 10^6 (2×10^5) ^{87}Rb atoms coexisting with 7.5×10^5 (3×10^4) ^{40}K atoms with a quantum degeneracy of about $T/T_F = 0.1$ ($T/T_F = 0.3$) was achieved in the Hamburg (Florence) experiment. The parameters of both experiments are summarized in Table 1. The distinct values for the interspecies s-wave scattering length a_{BF} employed to describe each experiment are worth a detailed explanation since this parameter is of great importance for the system, especially for the stability of the mixture against collapsing. An overview of different values for a_{BF} and their determination method along with a reference are shown in Table 2. A comparison of the incompatible values for a_{BF} shows the need of further investigation in this field.

Now we give an outline of the contents of the paper. At first, we develop in Section 2 a mean-field theory for an ultracold dilute gaseous boson-fermion mixture within the functional integral approach to many-body theory. By splitting the Bose fields into background fields and fluctuation fields, we derive an effective action of the Bose subsystem without integrating out the fermionic degrees of freedom. Its extremization at zero temperature yields two coupled equations of motion, one for the condensate wave function and another one for the Green function of the fermions. By evaluating the fermionic Green function for a stationary BEC within the semiclassical approximation, we obtain how the time-independent Gross-Pitaevskii equation for the condensate wave function is modified in such a mixture.

In Section 3 we apply the Thomas-Fermi approximation by neglecting the kinetic energy of the bosons and obtain an algebraic Gross-Pitaevskii equation. With the help of its solution we determine the density profiles of both components in a ^{87}Rb–^{40}K mixture, where the contact interaction is repulsive between the bosons and attractive between both components.

Finally, we investigate in Section 4 the stability of the Bose-Fermi mixture with respect to collapse by numerically evaluating the effective action for a trial Gaussian density profile of the condensate. We compare our results, which strongly depend on the value of the Bose-Fermi s-wave scattering length, with the experiments on ^{87}Rb–^{40}K mixtures in Hamburg and Florence. The good agreement of our theoretical results with the measurement in the Florence experiment allows us to fit a_{BF} which describes the Hamburg data quite well, but remains incompatible with the value used in Florence.

2 Derivation of Gross-Pitaevskii equation

In this section we summarize briefly the mean-field theory of boson-fermion mixtures [24,14] and derive within the functional integral formalism a coupled set of differential equations for the condensate wave function and the fermionic Green function.

2.1 Grand-Canonical partition function

We consider a dilute gaseous mixture of ultracold bosonic and fermionic atoms. In order to obtain quantum statistical quantities for such a Bose-Fermi mixture, we use the grand-canonical partition function in the functional integral formalism. Thus, we integrate over all possible Bose fields $\psi_B^*(\mathbf{x},\tau)$, $\psi_B(\mathbf{x},\tau)$ and Fermi fields $\psi_F^*(\mathbf{x},\tau)$, $\psi_F(\mathbf{x},\tau)$, which are weighted by a Boltzmann factor [14,32,33]:

$$\mathcal{Z} = \oint \mathcal{D}\psi_B^* \oint \mathcal{D}\psi_B \oint \mathcal{D}\psi_F^* \oint \mathcal{D}\psi_F e^{-\mathcal{A}[\psi_B^*,\psi_B,\psi_F^*,\psi_F]/\hbar}. \tag{1}$$

The complex fields $\psi_B^*(\mathbf{x},\tau)$, $\psi_B(\mathbf{x},\tau)$ represent the bosons and are periodic on the imaginary time interval $[0,\hbar\beta]$, whereas the fermions are described by Grassmann fields $\psi_F^*(\mathbf{x},\tau)$, $\psi_F(\mathbf{x},\tau)$ which are antiperiodic on this interval:

$$\psi^*(\mathbf{x},\hbar\beta) = \epsilon\psi^*(\mathbf{x},0), \quad \psi(\mathbf{x},\hbar\beta) = \epsilon\psi(\mathbf{x},0). \tag{2}$$

Here $\epsilon = \pm 1$ holds for bosons and fermions, respectively. The total Euclidean action of a Bose-Fermi mixture consists of three parts:

$$\mathcal{A}[\psi_B^*,\psi_B,\psi_F^*,\psi_F] = \mathcal{A}_B[\psi_B^*,\psi_B] + \mathcal{A}_F[\psi_F^*,\psi_F] + \mathcal{A}_{BF}[\psi_B^*,\psi_B,\psi_F^*,\psi_F]. \tag{3}$$

Table 1. List of parameters of the experiments with a ^{87}Rb–^{40}K boson-fermion mixture. The values are taken from the experiments in Hamburg [6] and in Florence [4,10,27].

	Hamburg Experiment	Florence Experiment
mass of ^{87}Rb atom	$m_B = 14.43 \times 10^{-26}$ kg	
mass of ^{40}K atom	$m_F = 6.636 \times 10^{-26}$ kg	
s-wave scattering length (bosons ↔ bosons)	$a_{BB} = (5.238 \pm 0.002)$ nm	
s-wave scattering length (bosons ↔ fermions)	$a_{BF} = -15.0$ nm	$a_{BF} = (-20.9 \pm 0.8)$ nm
radial trap frequency (bosons)	$\omega_{B,r} = 2\pi \times 257$ Hz	$\omega_{B,r} = 2\pi \times 215$ Hz
axial trap frequency (bosons)	$\omega_{B,z} = 2\pi \times 11.3$ Hz	$\omega_{B,z} = 2\pi \times 16.3$ Hz
radial trap frequency (fermions)	$\omega_{F,r} = 2\pi \times 379$ Hz	$\omega_{F,r} = 2\pi \times 317$ Hz
axial trap frequency (fermions)	$\omega_{F,z} = 2\pi \times 16.7$ Hz	$\omega_{F,z} = 2\pi \times 24.0$ Hz
number of bosons	$N_B = 10^6$	$N_B = 2 \times 10^5$
number of fermions	$N_F = 7.5 \times 10^5$	$N_F = 3 \times 10^4$

Table 2. List of several published values of the s-wave scattering length between ^{87}Rb and ^{40}K including their determination method and their reference.

a_{BF}/a_{Bohr}	Method of determination	Reference (year)
-261^{+170}_{-159}	measurement of the elastic cross section for collisions between ^{41}K and ^{87}Rb in different temperature regimes and following mass scaling to the fermionic ^{40}K isotope	[28] (2002)
-330^{+160}_{-100}	measurement of the rethermalization time in the mixture in [4,10] after a selectively heating of ^{87}Rb	[4] (2002)
-410^{+81}_{-91}	measurement of the damping of the relative oscillations of ^{40}K and ^{87}Rb in a magnetic trap	[10] (2002)
-395 ± 15	mean-field analysis of the stability of the mixture in [4,10]	[27] (2003)
-281 ± 15	magnetic Feshbach spectroscopy of an ultracold mixture of ^{40}K and ^{87}Rb atoms	[29] (2004)
250 ± 30	cross dimensional thermal relaxation in a mixture of ^{40}K and ^{87}Rb atoms after a increase of the radial confinement of the magnetic trap, here only $\lvert a_{BF}/a_0 \rvert$	[30] (2004)
-284	mean-field analysis of the stability, based on [24], of the mixture in [6]	[6] (2006)
-205 ± 5	extensive magnetic Feshbach spectroscopy of an ultracold mixture of ^{40}K and ^{87}Rb atoms	[31] (2006)

The first term describes the bosonic component of the mixture:

$$\mathcal{A}_B[\psi_B^*,\psi_B] = \int_0^{\hbar\beta} d\tau \int d^3x \psi_B^*(\mathbf{x},\tau)\Big[\hbar\frac{\partial}{\partial\tau} - \frac{\hbar^2}{2m_B}\Delta + V_B(\mathbf{x}) - \mu_B + \frac{g_{BB}}{2}|\psi_B(\mathbf{x},\tau)|^2\Big]\psi_B(\mathbf{x},\tau). \quad (4)$$

It contains the Legendre transform, the kinetic energy, the external trap potential $V_B(\mathbf{x})$, the chemical potential μ_B to fix the boson number, and the strength $g_{BB} = 4\pi\hbar^2 a_{BB}/m_B$ of the contact interaction between two bosons with the s-wave scattering length a_{BB}. As we deal with a dilute gas, an interaction between more than two particles is negligible, and we can restrict ourselves to the short-range contact interaction. Since the Pauli principle forbids fermions in the same hyperfine state to be close together and therefore to collide via contact interaction, we can write the corresponding action term for the fermionic component of the mixture as

$$\mathcal{A}_F[\psi_F^*,\psi_F] = \int_0^{\hbar\beta} d\tau \int d^3x \psi_F^*(\mathbf{x},\tau)\Big[\hbar\frac{\partial}{\partial\tau} - \frac{\hbar^2}{2m_F}\Delta + V_F(\mathbf{x}) - \mu_F\Big]\psi_F(\mathbf{x},\tau), \quad (5)$$

where $V_F(\mathbf{x})$ and μ_F denote the external trap potential and the chemical potential for fermions. As we assume a situation, where the bosonic and fermionic atoms cannot be transformed into each other, each of both species has its own chemical potential. The last term of the Euclidean action (3)

$$\mathcal{A}_{BF}[\psi_B^*,\psi_B,\psi_F^*,\psi_F] = g_{BF}\int_0^{\hbar\beta} d\tau \int d^3x |\psi_B(\mathbf{x},\tau)|^2|\psi_F(\mathbf{x},\tau)|^2 \quad (6)$$

describes the contact interaction between bosons and fermions, where its strength g_{BF} is related to the s-wave scattering lengths a_{BF} via [34,35]

$$g_{BF} = 2\pi\hbar^2 a_{BF}\frac{m_B + m_F}{m_B m_F}. \quad (7)$$

2.2 Background method

In order to account for the fact that the bosons in the mixture can condense, we apply the background method of field theory [33,36,37] and split the bosonic fields $\psi_B^*(\mathbf{x},\tau)$, $\psi_B(\mathbf{x},\tau)$ into two parts:

$$\psi_B^*(\mathbf{x},\tau) = \Psi_B^*(\mathbf{x},\tau) + \delta\psi_B^*(\mathbf{x},\tau),$$
$$\psi_B(\mathbf{x},\tau) = \Psi_B(\mathbf{x},\tau) + \delta\psi_B(\mathbf{x},\tau). \quad (8)$$

The first part represents the background fields $\Psi_B^*(\mathbf{x},\tau)$, $\Psi_B(\mathbf{x},\tau)$ whose absolute square is identified with the density of the condensed bosons. The second part consists

of the fluctuation fields $\delta\psi_B^*(\mathbf{x},\tau)$, $\delta\psi_B(\mathbf{x},\tau)$ of the Bose gas describing the excited bosons, which are not in the ground state. Using the decomposition (8), we expand the Euclidean action (3) in a functional Taylor series with respect to the Bose fields $\psi_B^*(\mathbf{x},\tau)$, $\psi_B(\mathbf{x},\tau)$ around the background fields $\Psi_B^*(\mathbf{x},\tau)$, $\Psi_B(\mathbf{x},\tau)$. In this work we restrict ourselves to the Gross-Pitaevskii theory, i.e. we consider the Euclidean action $\mathcal{A}$ only up to the zeroth order in the fluctuation fields $\delta\psi_B^*(\mathbf{x},\tau)$, $\delta\psi_B(\mathbf{x},\tau)$ which is equivalent to evaluate the Euclidean action (3) at the background fields: $\mathcal{A}[\Psi_B^* + \delta\psi_B^*, \Psi_B + \delta\psi_B, \psi_F^*, \psi_F] \approx \mathcal{A}[\Psi_B^*, \Psi_B, \psi_F^*, \psi_F]$. Thus, the bosonic functional integration in equation (1), whose integration measure transforms according $\mathcal{D}\psi_B^*(\mathbf{x},\tau) = \mathcal{D}\delta\psi_B^*(\mathbf{x},\tau)$ and $\mathcal{D}\psi_B(\mathbf{x},\tau) = \mathcal{D}\delta\psi_B(\mathbf{x},\tau)$, can be dropped. In this way we obtain for the effective action $\Gamma[\Psi_B^*,\Psi_B] = -\ln\mathcal{Z}[\Psi_B^*,\Psi_B]/\beta$ the result

$$\Gamma[\Psi_B^*,\Psi_B] = \frac{1}{\hbar\beta}\mathcal{A}_B[\Psi_B^*,\Psi_B] - \frac{1}{\beta}\ln\mathcal{Z}_F[\Psi_B^*,\Psi_B], \quad (9)$$

where

$$\mathcal{Z}_F[\Psi_B^*,\Psi_B] = \oint\mathcal{D}\psi_F^*\oint\mathcal{D}\psi_F e^{-\mathcal{A}_{F,\mathrm{eff}}[\Psi_B^*,\Psi_B,\psi_F^*,\psi_F]/\hbar} \quad (10)$$

represents the functional integral over the Fermi fields resulting in a pure functional of the Bose background fields $\Psi_B^*(\mathbf{x},\tau)$, $\Psi_B(\mathbf{x},\tau)$. The effective Euclidean action $\mathcal{A}_{F,\mathrm{eff}}[\Psi_B^*,\Psi_B,\psi_F^*,\psi_F]$ depending on the Fermi fields $\psi_F^*(\mathbf{x},\tau)$, $\psi_F(\mathbf{x},\tau)$ is summarized by

$$\mathcal{A}_{F,\mathrm{eff}}[\Psi_B^*,\Psi_B,\psi_F^*,\psi_F] = \int_0^{\hbar\beta}d\tau\int d^3x\psi_F^*(\mathbf{x},\tau)\Big[\hbar\frac{\partial}{\partial\tau} + \hat{H}_{F,\mathrm{eff}}(\mathbf{x},\tau) - \mu_F\Big]\psi_F(\mathbf{x},\tau), \quad (11)$$

where the effective one-particle Hamilton operator for fermions reads:

$$\hat{H}_{F,\mathrm{eff}}(\mathbf{x},\tau) = -\frac{\hbar^2}{2m_F}\Delta + V_F(\mathbf{x}) + g_{BF}|\Psi_B(\mathbf{x},\tau)|^2. \quad (12)$$

2.3 Coupled equations of motion

The grand-canonical free energy $\mathcal{F}$ is the extremum of the effective action $\Gamma[\Psi_B^*,\Psi_B]$ with respect to the background fields $\Psi^*(\mathbf{x},\tau)$, $\Psi(\mathbf{x},\tau)$. Using equations. (4) and (9)–(12), this yields the time-dependent Gross-Pitaevskii equation:

$$\Big[\hbar\frac{\partial}{\partial\tau} - \frac{\hbar^2}{2m_B}\Delta + V_B(\mathbf{x}) - \mu_B + g_{BB}|\Psi_B(\mathbf{x},\tau)|^2 - g_{BF}G_F(\mathbf{x},\tau;\mathbf{x},\tau)\Big]\Psi_B(\mathbf{x},\tau) = 0, \quad (13)$$

where the fermionic two-point function is defined as follows:

$$G_F(\mathbf{x},\tau;\mathbf{x}',\tau') \equiv \frac{1}{\mathcal{Z}_F[\Psi_B^*,\Psi_B]}\oint\mathcal{D}\psi_F^* \times\oint\mathcal{D}\psi_F\psi_F(\mathbf{x},\tau)\psi_F^*(\mathbf{x}',\tau')e^{-\mathcal{A}_{F,\mathrm{eff}}[\Psi_B^*,\Psi_B,\psi_F^*,\psi_F]/\hbar}. \quad (14)$$

This imaginary time-dependent nonlinear Schrödinger equation (13) of the condensate wave function $\Psi_B(\mathbf{x},\tau)$ represents a partial differential equation, where the nonlinear terms are due to both interactions. The last term results from the boson-fermion interaction, whereas the other terms have the conventional Gross-Pitaevskii form for a condensate [38,39]. The fermionic two-point function is at the same time a Green function for the fermion fields, thus, it obeys the linear inhomogeneous Schrödinger equation for fermions

$$\Big[\hbar\frac{\partial}{\partial\tau} + \hat{H}_{F,\mathrm{eff}}(\mathbf{x},\tau) - \mu_F\Big]G_F(\mathbf{x},\tau;\mathbf{x}',\tau') = \hbar\delta(\mathbf{x}-\mathbf{x}')\delta^{(a)}(\tau-\tau'), \quad (15)$$

where the inhomogeneity consists of the delta function in space and the antiperiodic repetitive delta function in imaginary time

$$\delta^{(a)}(\tau-\tau') = \sum_{n=-\infty}^{\infty}(-1)^n\delta(\tau-\tau'+n\hbar\beta). \quad (16)$$

The Gross-Pitaevskii equation (13) for the condensate and the inhomogeneous Schrödinger equation (15) for fermions form a set of coupled equations in imaginary time. Therein the condensate wave function $\Psi_B(\mathbf{x},\tau)$ in the Gross-Pitaevskii equation (13) is modified by the fermionic Green function $G_F(\mathbf{x},\tau;\mathbf{x},\tau)$ and, vice versa, the condensate wave function $\Psi_B(\mathbf{x},\tau)$ influences the fermionic Green function $G_F(\mathbf{x},\tau;\mathbf{x}',\tau')$ in the inhomogeneous Schrödinger equation (15). A Wick rotation $\tau = it$ and the omission of the chemical potentials in equations (13) and (15) leads to two coupled equations of motion in real time, which describe the dynamics in the Bose-Fermi mixture.

2.4 Fermionic Green function

In the following we obtain an approximative solution for the fermionic Green function $G_F(\mathbf{x},\tau;\mathbf{x}',\tau')$. To this end we restrict ourselves to a stationary BEC so that the imaginary time-dependent Gross-Pitaevskii equation (13) reduces to

$$\Big[-\frac{\hbar^2}{2m_B}\Delta + V_B(\mathbf{x}) - \mu_B + g_{BB}|\Psi_B(\mathbf{x})|^2 - g_{BF}G_F(\mathbf{x},\tau;\mathbf{x},\tau)\Big]\Psi_B(\mathbf{x}) = 0, \quad (17)$$

$$G_F(\mathbf{x},\tau;\mathbf{x}',\tau') = \int \frac{d^3k}{(2\pi)^3} e^{i\mathbf{k}\times(\mathbf{x}-\mathbf{x}')} \frac{\Theta(\tau-\tau')e^{-[E(\mathbf{k},(\mathbf{x}+\mathbf{x}')/2)-\mu_F](\tau-\tau'-\hbar\beta/2)/\hbar} - \Theta(\tau'-\tau)e^{-[E(\mathbf{k},(\mathbf{x}+\mathbf{x}')/2)-\mu_F](\tau-\tau'+\hbar\beta/2)/\hbar}}{2\cosh\beta[E(\mathbf{k},(\mathbf{x}+\mathbf{x}')/2)-\mu_F]/2}. \tag{22}$$

and the effective fermionic Hamiltonian (12) no longer depends explicitly on the imaginary time τ:

$$\hat{H}_{F,\mathrm{eff}}(\mathbf{x}) = -\frac{\hbar^2}{2m_F}\Delta + V_F(\mathbf{x}) + g_{BF}|\Psi_B(\mathbf{x})|^2. \tag{18}$$

Now we assume that both the fermionic trap potential $V_F(\mathbf{x})$ and the condensate wave function $\Psi_B(\mathbf{x})$ have only a weak spatial dependence so that the semiclassical approximation can be applied. Therein the eigenvalue problem

$$\hat{H}_{F,\mathrm{eff}}(\mathbf{x})\psi_{\mathbf{k}}(\mathbf{x}) = E(\mathbf{k},\mathbf{x})\psi_{\mathbf{k}}(\mathbf{x}) \tag{19}$$

is approximately solved by plane waves

$$\psi_{\mathbf{k}}(\mathbf{x}) = \frac{e^{i\mathbf{k}\times\mathbf{x}}}{(2\pi)^{3/2}} \tag{20}$$

and the semiclassical energy spectrum

$$E(\mathbf{k},\mathbf{x}) = \frac{\hbar^2\mathbf{k}^2}{2m_F} + V_F(\mathbf{x}) + g_{BF}|\Psi_B(\mathbf{x})|^2. \tag{21}$$

Thus, the semiclassical solution of equation (15) yields for the fermionic Green function

see equation (22) above.

The limit of equal imaginary times follows from $\tau' \downarrow \tau$:

$$G_F(\mathbf{x},\tau;\mathbf{x}',\tau) = -\int \frac{d^3k}{(2\pi)^3} \frac{e^{i\mathbf{k}\times(\mathbf{x}-\mathbf{x}')}}{e^{\beta[E(\mathbf{k},(\mathbf{x}+\mathbf{x}')/2)-\mu_F]}+1}. \tag{23}$$

Thus, the fermionic particle density $n_F(\mathbf{x}) = -G_F(\mathbf{x},\tau;\mathbf{x},\tau)$ is given by

$$n_F(\mathbf{x}) = \int \frac{d^3k}{(2\pi)^3} \frac{1}{e^{\beta[\hbar^2\mathbf{k}^2/2m_F-\tilde{\mu}_F(\mathbf{x})]}+1} \tag{24}$$

with the local chemical potential

$$\tilde{\mu}_F(\mathbf{x}) = \mu_F - V_F(\mathbf{x}) - g_{BF}|\Psi_B(\mathbf{x})|^2, \tag{25}$$

which represents the kinetic energy of the fermion in the highest energetic state, when it is located at the space point $\mathbf{x}$. In order to evaluate the integral (24) in momentum space, we apply spherical coordinates and the substitution $\varepsilon(k) = \hbar^2k^2/2m_F$:

$$n_F(\mathbf{x}) = \frac{1}{\Gamma(3/2)}\left(\frac{m_F}{2\pi\hbar^2}\right)^{3/2}\int_0^\infty \frac{d\varepsilon\varepsilon^{1/2}}{e^{\beta[\varepsilon-\tilde{\mu}_F(\mathbf{x})]}+1}. \tag{26}$$

In the low-temperature limit $T \downarrow 0$, the Sommerfeld expansion [40] of equation (26) yields in the lowest order

$$n_F(\mathbf{x}) = \kappa\Theta\left(\tilde{\mu}_F(\mathbf{x})\right)\tilde{\mu}_F^{3/2}(\mathbf{x}) \tag{27}$$

with the abbreviation $\kappa = (2m_F)^{3/2}/6\pi^2\hbar^3$. Finally, we insert the result for the fermionic particle density (27) into the Gross-Pitaevskii equation (17):

$$\Big[-\frac{\hbar^2}{2m_B}\Delta + V_B(\mathbf{x}) - \mu_B + g_{BB}|\Psi_B(\mathbf{x})|^2 + \kappa g_{BF}\Theta\left(\tilde{\mu}_F(\mathbf{x})\right)\tilde{\mu}_F^{3/2}(\mathbf{x})\Big]\Psi_B(\mathbf{x}) = 0. \tag{28}$$

Note that this stationary Gross-Pitaevskii equation (28) follows from extremizing the effective action

$$\Gamma[\Psi_B^*,\Psi_B] = \int d^3x\Big\{\Psi_B^*(\mathbf{x})\Big[-\frac{\hbar^2}{2m_B}\Delta + V_B(\mathbf{x}) - \mu_B + \frac{g_{BB}}{2}|\Psi_B(\mathbf{x})|^2\Big]\Psi_B(\mathbf{x}) - \frac{2}{5}\kappa\Theta(\tilde{\mu}_F(\mathbf{x}))\tilde{\mu}_F^{5/2}(\mathbf{x})\Big\} \tag{29}$$

with respect to $\Psi_B^*(\mathbf{x})$. This effective action can also be obtained from equations (4) and (9)–(12) by evaluating the fermionic functional integral (10) in the semiclassical approximation for a stationary BEC and by performing the Sommerfeld expansion in the low-temperature limit. Identifying the extremum of the effective action Γ with the grand-canonical free energy $\mathcal{F}$, the number of bosons and fermions are obtained from (29) via the normalization condition

$$N_j = -\frac{\partial\mathcal{F}}{\partial\mu_j} = \int d^Dx n_j(\mathbf{x}), \quad j = B,F, \tag{30}$$

where the particle densities of bosons and fermions read

$$n_B(\mathbf{x}) = |\Psi_B(\mathbf{x})|^2, \tag{31}$$

$$n_F(\mathbf{x}) = \kappa\Theta\left(\tilde{\mu}_F(\mathbf{x})\right)\tilde{\mu}_F^{3/2}(\mathbf{x}). \tag{32}$$

3 Density profiles

In this section we solve the stationary Gross-Pitaevskii equation (28) in the Thomas-Fermi approximation in order to calculate the boson and the fermion density distribution for the parameters of the experiment in Hamburg [6]. There the ^{87}Rb–^{40}K boson-fermion mixture is confined in a three-dimensional rotationally symmetric harmonic trap

$$V_i(\mathbf{x}) = \frac{m_i}{2}\left(\omega_{i,r}^2r^2 + \omega_{i,z}^2z^2\right), \quad i = B,F, \tag{33}$$

where we use cylindrical coordinates $\{r,\phi,z\}$. The frequencies for both species are related by $\omega_{F,k} = \sqrt{m_B/m_F}\omega_{B,k}$ for $k = r,z$, so that $m_B\omega_{B,k}^2/2 = m_F\omega_{F,k}^2/2$.

3.1 Thomas-Fermi approximation

Assuming that the potential and interaction energy are larger than the kinetic energy, we can use the Thomas-Fermi approximation, where the kinetic term in the Gross-Pitaevskii equation can be neglected. With this approximation the Gross-Pitaevskii equation (28) reduces with the help of equations (31) and (32) to an algebraic equation with respect to the bosonic particle density $n_B(\mathbf{x})$ [41]:

$$V_B(\mathbf{x}) - \mu_B + g_{BB} n_B(\mathbf{x}) + g_{BF} n_F(\mathbf{x}) = 0. \quad (34)$$

The last term in equation (34) stands for the fermionic particle density

$$n_F(\mathbf{x}) = \kappa\Theta\left(\mu_F - V_F(\mathbf{x}) - g_{BF} n_B(\mathbf{x})\right) \times \left[\mu_F - V_F(\mathbf{x}) - g_{BF} n_B(\mathbf{x})\right]^{3/2}, \quad (35)$$

which modulates the bosonic density profile $n_B(\mathbf{x})$ and vice versa.

3.2 Vanishing boson-fermion interaction

Now we discuss the special case of vanishing boson-fermion interaction $g_{BF} \to 0$, where we mark all quantities with the upper index (0). On the one hand, equation (34) reduces then to the well-known particle density of a pure BEC in the Thomas-Fermi approximation

$$n_B^{(0)}(\mathbf{x}) = \frac{1}{g_{BB}}\Theta\left(\mu_B^{(0)} - V_B(\mathbf{x})\right)\left[\mu_B^{(0)} - V_B(\mathbf{x})\right], \quad (36)$$

provided that $g_{BB} > 0$. In case of an attractive interacting BEC with negative g_{BB}, the third term in equation (34) cannot be balanced in the trap center at $\mathbf{x} = \mathbf{0}$ by the remaining chemical potential $\mu_B^{(0)}$ leading to a collapse of the BEC. The particle density (35) of fermions, on the other hand, becomes independent of that of bosons:

$$n_F^{(0)}(\mathbf{x}) = \kappa\Theta\left(\mu_F^{(0)} - V_F(\mathbf{x})\right)\left[\mu_F^{(0)} - V_F(\mathbf{x})\right]^{3/2}. \quad (37)$$

Thus, the clouds of the BEC and the Fermi gas coexist undisturbed from each other. Setting the particle densities (36) and (37) zero yields the Thomas-Fermi-radii of the BEC and the Fermi cloud along the respective axes:

$$R_{i,k}^{(0)} = \sqrt{\frac{2\mu_i^{(0)}}{m_i\omega_{i,k}^2}}, \quad i = B, F. \quad (38)$$

The chemical potentials $\mu_B^{(0)}$ and $\mu_F^{(0)}$ are determined by the particle numbers N_B and N_F via the normalization (30):

$$\mu_B^{(0)} = \left(\frac{15 a_{BB} N_B}{\tilde{L}_B}\right)^{2/5} \frac{\hbar\tilde{\omega}_B}{2}, \quad \mu_F^{(0)} = (6N_F)^{1/3}\hbar\tilde{\omega}_F, \quad (39)$$

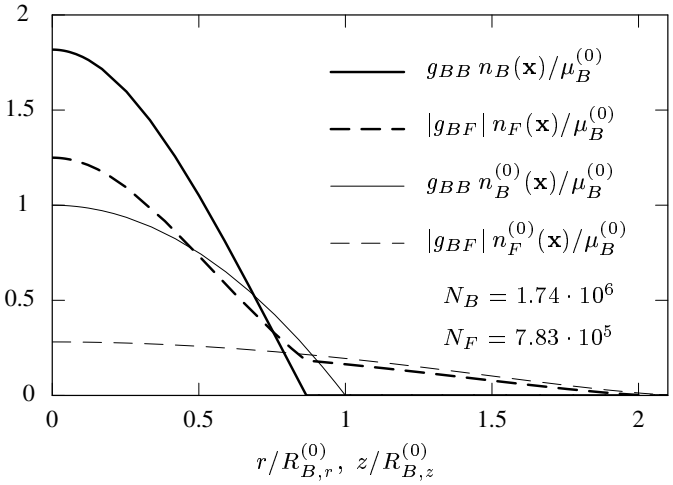

Fig. 1. Comparison of the dimensionless particle densities for bosons and for fermions between a disturbed mixture (thick lines) and an undisturbed BEC and Fermi gas (thin lines). The densities are plotted versus the coordinates r at the plane $z = 0$ and z at the line $r = 0$, respectively, in units of the Thomas-Fermi radii of the undisturbed BEC. The densities of the disturbed mixture are the solution of equations (34) and (35), whereas those of an undisturbed BEC and Fermi gas are given by equations (36) and (37), respectively, for an example of typical particle numbers N_B, N_F of the Hamburg experiment [6].

where $\tilde{L}_i = \sqrt{\hbar/m_i\tilde{\omega}_i}$ denotes the geometrical average of the oscillator lengths $L_{i,k} = \sqrt{\hbar/m_i\omega_{i,k}}$. Inserting the chemical potentials (39) into the respective particle densities (36) and (37), the maximum of the latter in the trap center results in

$$n_B^{(0)}(\mathbf{0}) = \frac{(15N_B)^{2/5}}{8\pi a_{BB}^{3/5}\tilde{L}_B^{12/5}}, \quad n_F^{(0)}(\mathbf{0}) = \frac{2N_F^{1/2}}{3^{1/2}\pi^2\tilde{L}_F^3}. \quad (40)$$

In the Thomas-Fermi approximation the BEC needs a non-vanishing repulsion between the bosons in order to prevent the density from becoming infinite or complex, which indicates a collapse of the BEC, whereas the quantum pressure in the noninteracting Fermi gas preserves the latter from a collapse. The maximum fermionic particle density increases faster with the particle number than the maximum bosonic particle density, whereas the latter depends not only on the oscillator length but also on a_{BB}, the parameter for the bosonic interaction strength. The particle densities of both species in an undisturbed BEC and Fermi gas are plotted for typical particle numbers N_B and N_F as thin lines in Figure 1.

3.3 Non-vanishing boson-fermion interaction

After having treated the case $g_{BF} = 0$ in the previous section, we now discuss the algebraic equation (34) for a BEC which interacts with fermions. In order to plot the corresponding bosonic and fermionic densities in Figure 1, we

insert the fermionic density (35) into the algebraic equation (34) and obtain:

$$V_B(\mathbf{x}) - \mu_B + g_{BB} n_B(\mathbf{x}) = - g_{BF}\kappa \left[\mu_F - V_F(\mathbf{x}) - g_{BF} n_B(\mathbf{x})\right]^{3/2}. \quad (41)$$

Squaring (41) leads to a cubic equation with respect to the condensate density $n_B(\mathbf{x})$:

$$n_B^3(\mathbf{x}) + \left\{\frac{g_{BB}^2}{\kappa^2 g_{BF}^5} - \frac{3[\mu_F - V_F(\mathbf{x})]}{g_{BF}}\right\} n_B^2(\mathbf{x}) + \left\{\frac{2g_{BB}[V_B(\mathbf{x}) - \mu_B]}{\kappa^2 g_{BF}^5} + \frac{3[\mu_F - V_F(\mathbf{x})]^2}{g_{BF}^2}\right\} n_B(\mathbf{x}) + \frac{[V_B(\mathbf{x}) - \mu_B]^2}{\kappa^2 g_{BF}^5} - \frac{[\mu_F - V_F(\mathbf{x})]^3}{g_{BF}^3} = 0, \quad (42)$$

It is of the form

$$x^3 + ax^2 + bx + c = 0 \quad (43)$$

with real coefficients a, b, c and its three solutions x_1, x_2, x_3 can be found with the help of the Cardanian formula [42]. The first solution x_1 remains always real, whereas the other solutions x_2 and x_3 are either real for

$$\left[-\frac{a^2}{9} + \frac{b}{3}\right]^3 \leq -\left[-\frac{a^3}{27} + \frac{ab}{6} - \frac{c}{2}\right]^2 \quad (44)$$

or conjugate complex otherwise. Although all three solutions obey the cubic equation (43), i.e. equation (42), only the last solution x_3 turns out to satisfy the algebraic equation (41). Inserting the two other solutions into the algebraic equation yields the right value but opposite signs on both sides of the algebraic equation (41). The reason is that equation (41) represents the root of the cubic equation (42), therefore an equation of the order 3/2, which reduces the number of possible solutions.

The resulting particle densities for both species are plotted as thick lines in Figure 1 for typical particle numbers N_B and N_F using the experimental parameters in Table 1. In order to determine the solution outside the BEC, especially the particle density of fermions, we must not forget the origin of the algebraic equation (34) from the Gross-Pitaevskii equation (28). Although the solution $n_B(\mathbf{x})$ becomes negative outside the BEC, we have to set it equal zero there, as the density must be positive by definition. Thus, the condensate wave function $\Psi_B(\mathbf{x})$ becomes also zero outside the BEC and fulfills the Gross-Pitaevskii equation (28) in a trivial way regardless of the expression inside the brackets, which is, apart from the neglected kinetic energy term, the algebraic equation (34). Hence, the fermionic particle density outside the BEC is described by equation (35) with $n_B(\mathbf{x}) = 0$ without obeying the algebraic equation (34).

The particle density of the BEC in the Thomas-Fermi approximation can be written in the following form:

$$n_B(\mathbf{x}) = \frac{1}{g_{BB}}\left[\mu_B - V_B(\mathbf{x}) - g_{BF} n_F(\mathbf{x})\right]. \quad (45)$$

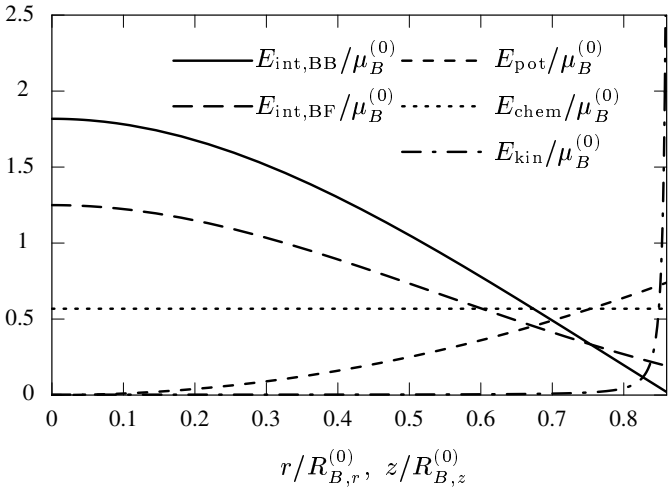

Fig. 2. Comparison of the kinetic energy $E_{\mathrm{kin}} = -\hbar^2\Delta\Psi_B(\mathbf{x})/(2m_B\Psi_B(\mathbf{x}))$ of a boson, with its remaining energies, namely the intraspecies interaction energy $E_{\mathrm{int,BB}} = g_{BB}n_B(\mathbf{x})$, the interspecies interaction energy $E_{\mathrm{int,BF}} = |g_{BF}|n_F(\mathbf{x})$, the potential energy $E_{\mathrm{pot}} = V_B(\mathbf{x})$ due to the trap and the chemical potential $E_{\mathrm{chem}} = \mu_B$. All energies are related to the value $\mu_B^{(0)}$ of the potential energy at the boundary of the undisturbed BEC cloud and are plotted versus the coordinates r and z within the BEC cloud for the situation in Figure 1.

From the fermionic particle density (35) we deduce that its maximum occurs in the trap center $\mathbf{x} = \mathbf{0}$ due to the negative g_{BF}. Thus, the BEC possesses its largest density also in the trap center. In other words, the particle densities of both species intensify each other in the overlapping region due to the strong attraction between bosons and fermions as is shown in Figure 1. With increasing distance from the trap center both densities (35) and (45) decrease quickly within their overlap due to the interspecies interaction terms and due to the increasing trap potentials, whereas outside of the overlap only the latter reason is responsible for their decreasing. This behavior is shown in Figure 1 for the Hamburg experiment. Which of both clouds has the larger extension depends on the particle numbers N_B and N_F and therefore on the chemical potentials μ_B and μ_F. Usually, the BEC is surrounded by the Fermi gas unless $N_B \gg N_F$. Both chemical potentials, which represent the total energy of a particle of the corresponding species, are smaller compared with $\mu_B^{(0)}$ and $\mu_F^{(0)}$ of the undisturbed BEC and Fermi gas, since the particles possess, besides the neglected kinetic energy, the potential energy due to the trap and the intraspecies interaction energy an additional negative interaction energy due to the interspecies interaction. Figure 2 shows these energies of a boson in units of $V_B(R_{B,r}, 0) = V_B(0, R_{B,z}) = \mu_B^{(0)}$ for the Hamburg experiment, where we see that $\mu_B \approx 0.6\mu_B^{(0)}$. These reduced chemical potentials lead to decreasing Thomas-Fermi radii for both species. Indeed, one can see in Figure 1 a reduction of the Thomas-Fermi radii of the BEC to $R_{B,k} \approx 0.8R_{B,k}^{(0)}$. Hence the attractive interaction

between both species leads to an additional confinement of both the BEC and the Fermi gas within their overlap.

A direct quantitative comparison with the density of the experimental probe is not possible since a measurement of the density in the trap fails due to the smallness of the probe. Only after the expansion of the probe, when the trap potential was suddenly switched off, its density can be measured taking the absorption image of the optical density of ^{87}Rb and ^{40}K. This would allow to compare the densities only qualitatively, since the density in the probe is changed due to both the ballistic expansion and the dynamics in the probe.

3.4 Validity of Thomas-Fermi approximation

In order to check the validity of the Thomas-Fermi approximation, we have plotted in Figure 2 the kinetic energy of a boson

$$E_{\rm kin} = \frac{-\hbar^2 \Delta \Psi_B(\mathbf{x})}{2m_B \Psi_B(\mathbf{x})} \tag{46}$$

in units of the value $\mu_B^{(0)}$ of the potential energy at the boundary of the undisturbed BEC. The kinetic energy is, indeed, negligible in a wide bulk range from the trap center to just before the boundary of the disturbed BEC. Thus, the Thomas-Fermi approximation gives very accurate results except in the outermost 10% of the Thomas-Fermi radii. The kinetic energy diverges at the BEC boundary because the condensate wave function $\Psi_B(\mathbf{x})$, which represents the square root of the particle density $n_B(\mathbf{x})$, occurs due to the Laplacian derivative in equation (46) in the denominator, which becomes zero at the BEC boundary. It is obvious that the proper solution of the Gross-Pitaevskii equation (28) would match the one of the algebraic equation (34) from the trap center to just before the BEC boundary, where it tends smoothly to zero, thus improving the sharp bend in the graph of the fermionic particle density there to be smooth.

3.5 Complex solutions

As already discussed in Section 3.3, the solution $n_B(\mathbf{x})$ of the algebraic equation (34) does not always remain real by varying the chemical potentials μ_B and μ_F. From the condition (44) we extract a straight line in the μ_B, μ_F-plane

$$\mu_F = \frac{4g_{BB}^2}{27\kappa^2 g_{BF}^4} + \frac{g_{BF}}{g_{BB}}\mu_B, \tag{47}$$

which separates the half plane with a complex solution from that with a real solution. This situation is depicted for the Hamburg experiment in Figure 3a. Due to the results of the subsequent Section 4, we can associate the complex solution to an instability of the mixture with respect to collapse. Figures 3b–d demonstrate the change of the density profiles $n_B(\mathbf{x})$ and $n_F(\mathbf{x})$ on the road from stability to instability by increasing the particle numbers with $\Delta N_B \approx 1.8 \times 10^5$ and $\Delta N_F \approx 3 \times 10^4$ each. The respective pairs (μ_B, μ_F) lie on the dashed line, which is arranged perpendicular to the critical solid line in Figure 3a, so for Figure 3b just below the critical line, for Figure 3c on, and for Figure 3d just above. Figure 3b shows a stable configuration, Figure 3c is on the boundary between stable and unstable where the densities pile up at the trap center to a peak, and in Figure 3d the real part of the densities is chopped off at the trap center, so that there an imaginary part of both densities occurs. This imaginary part starts to appear simultaneously for both components at the density maximum $\mathbf{x} = \mathbf{0}$ and grows in magnitude and in extension out of the trap center with increasing N_B and N_F. Such an anomaly in the densities was observed in the Hamburg experiment, where the evolution of an overcritical mixture is shown in Figure 1 of reference [6].

4 Stability against collapse

Here we determine the stability border both within the Thomas-Fermi approximation and, in a separate variational calculation, beyond the Thomas-Fermi approximation. The stability border turns out to depend strongly on the value of the interspecies s-wave scattering length. Therefore, comparing our theoretical results with the experimental measurements allows to extract a trustworthy value for this crucial s-wave scattering length.

4.1 Thomas-Fermi approximation

In Section 3.5 we described in detail the behavior of the particle densities $n_B(\mathbf{x})$ and $n_F(\mathbf{x})$ as the solution of the stationary Gross-Pitaevskii equation within the Thomas-Fermi approximation for varying particle numbers N_B and N_F. We assigned the emergence of a complex density to a loss of the stability against collapse and found a border in form of a line in the (μ_B, μ_F)-plane, which separates the stable and unstable regions as shown in Figure 3a. In order to obtain a stability diagram in the (N_B, N_F)-plane, we have evaluated the corresponding particle numbers from the chemical potentials by integrating out the respective particle densities according to the normalization condition (30). The result for the Hamburg and the Florence experiment is given by the dot-dashed line in Figures 4 and 5, respectively. Mixtures with particle number pairs (N_B, N_F) below this line are stable whereas particle number pairs above the line indicate an unstable mixture tending to collapse. The critical particle numbers of both species behave, roughly spoken, inversely proportional to each other in a wide range. Whereas the critical number of bosons $N_{B\rm crit}$ tends to zero when the number of fermions increases, the critical number of fermions $N_{F\rm crit}$ remains finite and constant when the number of bosons is enlarged. This situation, where the line in the stability diagram becomes vertical, happens when the BEC cloud becomes so large that it surrounds the Fermi gas. This defines a minimal number of fermions $N_{F,\rm min}$ below which the mixture remains stable irrespective of the number of bosons N_B.

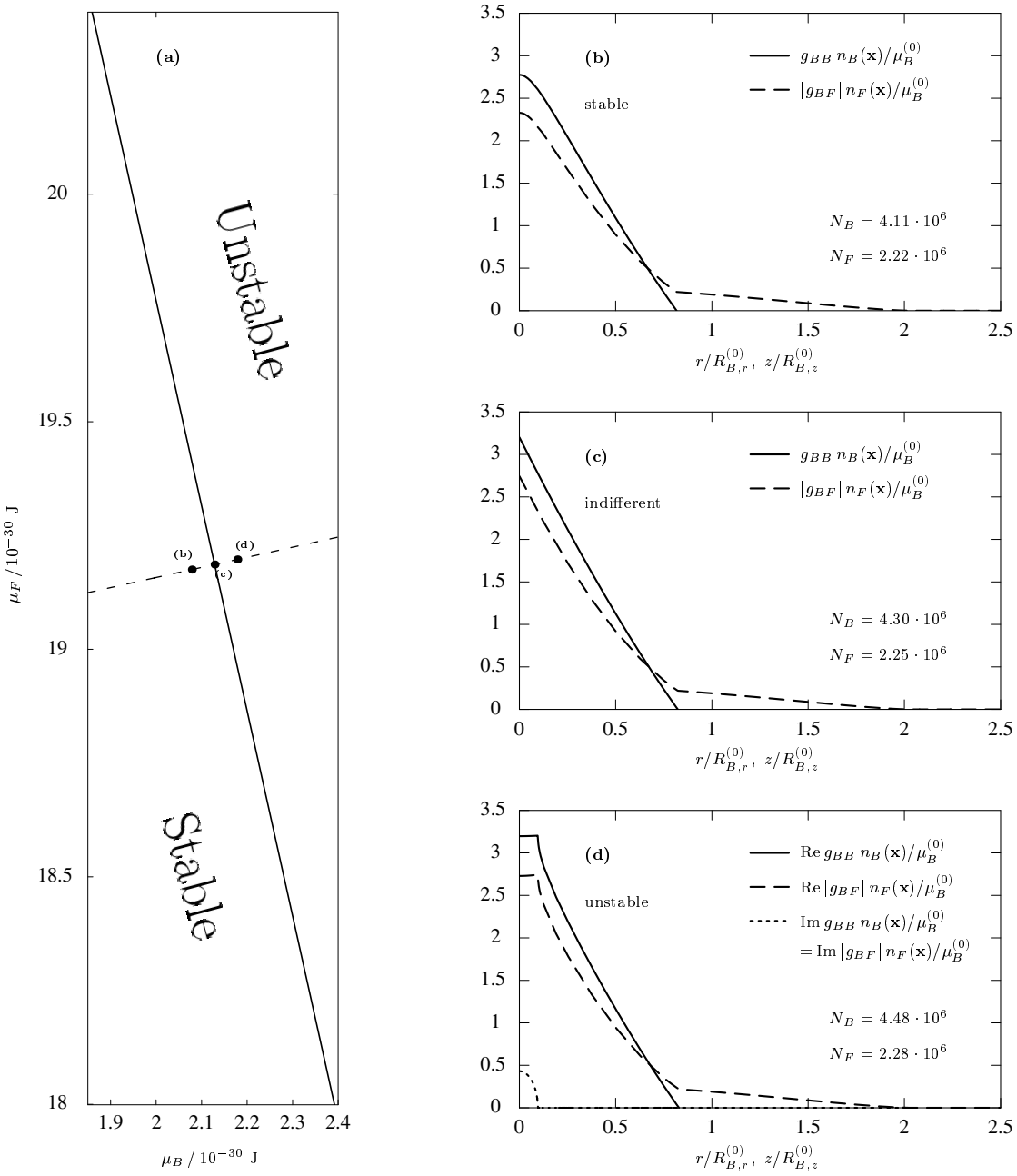

Fig. 3. (a) Stability diagram with respect to the chemical potentials. The solid line separates the stable region on the left from the unstable region on the right according to equation (47). The pictures (b)–(d) show a sequence how the bosonic and fermionic particle densities versus the coordinates r at the plane $z = 0$ and z at the line $r = 0$, respectively, change on the road from stability to instability. The (μ_B, μ_F)-pairs belonging to (b)–(d) are located on the dashed line in (a) and are equally spaced $\Delta\mu_B = 5 \times 10^{-32}$ J apart giving rise to particle number differences of about $\Delta N_B \approx 1.8 \times 10^5$ and $\Delta N_F \approx 3 \times 10^4$, respectively.

In order to estimate $N_{F,\min}$, we have to integrate the fermionic particle density (35) by taking into account the stability condition (47) when solving the algebraic equation (41) for the condensate density $n_B(\mathbf{x})$. In this way we find that the fermionic particle density (35) does not explicitly depend on both chemical potentials μ_F and μ_B. A numerical evaluation for the Hamburg (Florence) experiment yields $N_{F,\min} = 9,99 \times 10^5$ ($N_{F,\min} = 1,08 \times 10^4$) in accordance with the dot-dashed instability line shown in Figure 4 (Fig. 5).

4.2 Variational method

Another approach to determine the stability border for a ^{87}Rb–^{40}K mixture is based on extremizing the grand-canonical free energy (29) with the local chemical potential (25). In contrast to the Thomas-Fermi approximation

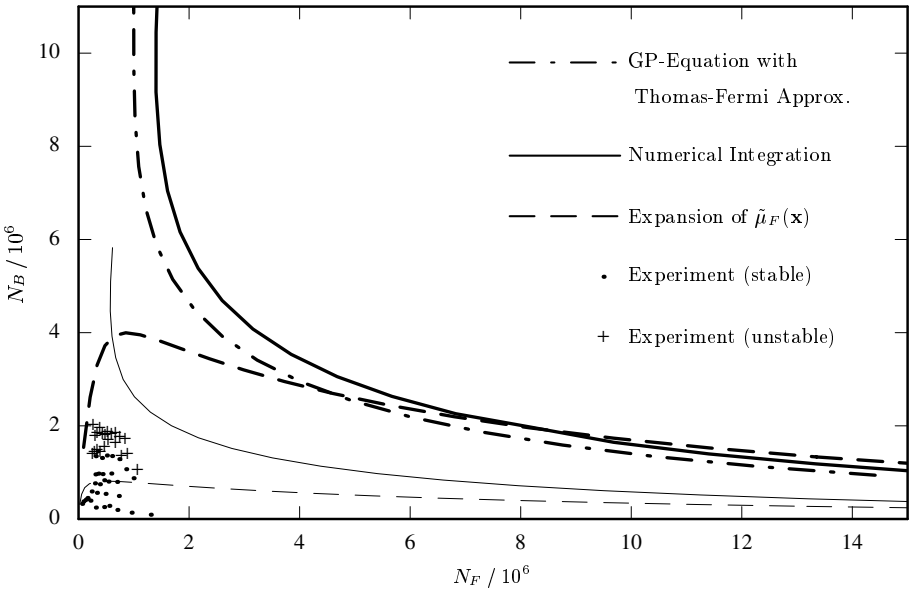

Fig. 4. Stability diagram for the ^{87}Rb–^{40}K mixture of the Hamburg experiment. The particle number pairs (N_B, N_F) below a certain line belong to a stable mixture whereas those above the line indicate an unstable mixture tending to collapse. The thin lines correspond to the quantum mechanical limit with the ratio $\lambda_{\mathrm{QM}} = \omega_z/\omega_r$ and the thick lines represent the Thomas-Fermi limit with the ratio $\lambda_{\mathrm{TF}} = (\omega_z/\omega_r)^2$. The points are obtained in the experiment by analyzing decay series in various particle number regimes and are assigned to stable mixtures (dots) and to unstable mixtures (crosses) [6].

in Section 4.1, this approach takes into account the kinetic energy of the condensed atoms. But instead of varying the condensate wave function $\Psi_B(\mathbf{x})$ in the grand-canonical free energy (29), which leads to the Gross-Pitaevskii equation as described in Section 2.4, we use the ground-state wave function of a three-dimensional anisotropic harmonic oscillator

$$\Psi_B(\mathbf{x}) = \sqrt{\frac{N_B}{\pi^{3/2}\alpha^3\tilde{L}_B^3}}\exp\left\{-\sum_{k=1}^{3}\frac{x_k^2}{2\alpha^2 L_{B,k}^2}\right\} \qquad (48)$$

as a test function with variational widths $\alpha L_{B,k}$. The dimensionless factor α, which scales the oscillator lengths of the Gaussian function (48), serves as a variational parameter, which extremizes the free energy (29). The test function is normalized to N_B bosons and obeys for $\alpha = 1$ the Gross-Pitaevskii equation for a trapped noninteracting BEC:

$$\left[-\frac{\hbar^2}{2m_B}\Delta + V_B(\mathbf{x}) - \mu_B\right]\Psi_B(\mathbf{x}) = 0. \qquad (49)$$

Here we assume that the condensate wave function $\Psi_B(\mathbf{x})$ has, also in case of intraspecies and interspecies two-particle interactions, qualitatively the shape of a Gaussian curve, as one can read off from Figure 1. Using cylindrical coordinates $\{r, \phi, z\}$, the test function (48) reads

$$\Psi_B(\mathbf{x}) = \sqrt{\frac{N_B\lambda^{1/2}}{\pi^{3/2}\alpha^3 L_{B,r}^3}}\exp\left\{-\frac{r^2+\lambda z^2}{2\alpha^2 L_{B,r}^2}\right\}. \qquad (50)$$

Beside a uniform variation of the widths $\alpha L_{B,k}$ by the factor α, we have to consider that the ratio $\lambda = (L_{B,z}/L_{B,r})^2$ could also change due to the interactions. In order to include this, we perform the calculation with two different ratios. On the one hand we use $\lambda_{\mathrm{QM}} = \omega_z/\omega_r$ which stands for the limit of vanishing interactions $g_{BB} \to 0$ and $g_{BF} \to 0$ and reflects the proper ratio of the oscillator lengths in the ground-state wave function of the quantum-mechanical harmonic oscillator (49). On the other hand, we set $\lambda_{\mathrm{TF}} = (\omega_z/\omega_r)^2$, which represents the Thomas-Fermi limit of negligible kinetic energy due to strong intraspecies and interspecies interaction. Inserting the test function (50) into the grand canonical free energy (29) reduces the latter from the functional $\mathcal{F}[\Psi_B^*, \Psi_B]$ to a function $\mathcal{F}(\alpha)$ of the parameter α. As the test function (50) is normalized independent of μ_B, the latter plays no longer a role in $\mathcal{F}(\alpha)$ and shifts the free energy only by a constant value. On the other hand, the fermionic chemical potential μ_F is needed for evaluating the respective fermion number N_F by integrating out the fermionic particle density (35) according to the normalization (30). The dependence of the grand-canonical free energy $\mathcal{F}(\alpha)$ on the variational parameter α for given chemical potentials μ_B and μ_F is shown in Figure 6 for several boson numbers N_B. For $N_B < N_{B\mathrm{crit}}$ the free energy $\mathcal{F}(\alpha)$ possesses a local minimum which corresponds to a metastable state of the mixture. The condensate wave function $\Psi_B(\mathbf{x})$ has finite equilibrium widths $\alpha_{\mathrm{eq}} L_{B,k}$, where α_{eq} denotes the parameter at the local minimum. When the boson number exceeds the critical value, i.e. $N_B > N_{B\mathrm{crit}}$, the local minimum disappears so that the widths tend to zero in order to minimize $\mathcal{F}(\alpha)$. Just this happens when the mixture collapses. Thus, the border between stability and instability is given by the condition

$$N_B = N_{B\mathrm{crit}} \Leftrightarrow \left.\frac{d\mathcal{F}(\alpha)}{d\alpha}\right|_{\alpha=\alpha_{\mathrm{crit}}} = \left.\frac{d^2\mathcal{F}(\alpha)}{d\alpha^2}\right|_{\alpha=\alpha_{\mathrm{crit}}} = 0, \qquad (51)$$

i.e. $\mathcal{F}(\alpha)$ has a point of inflexion at $\alpha = \alpha_{\mathrm{crit}}$. The appearance of the local minimum arises from the competition between the positive first three terms of the grand-canonical

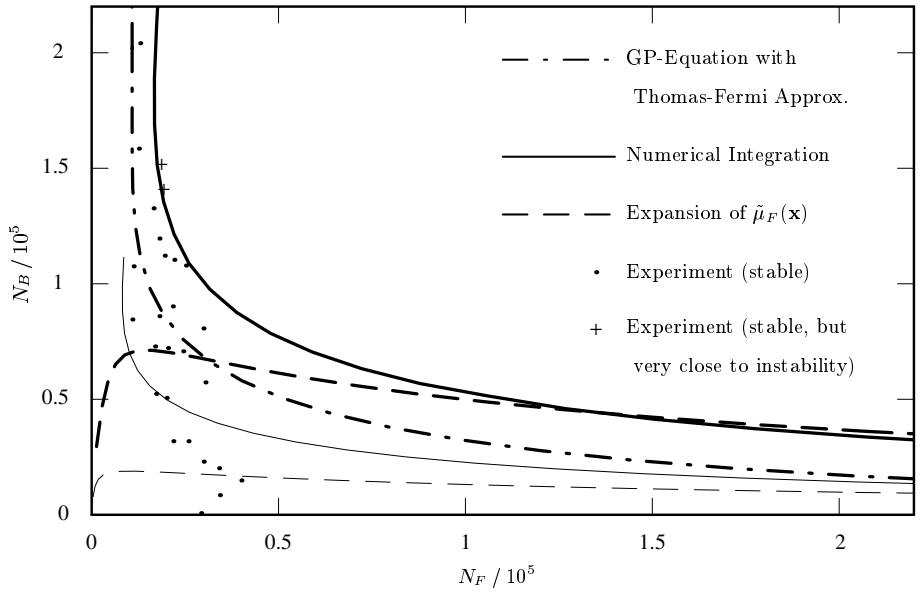

Fig. 5. Stability diagram for the ^{87}Rb–^{40}K mixture of the Florence experiment. The particle number pairs (N_B, N_F) below a certain line belong to a stable mixture whereas those above the line indicate an unstable mixture tending to collapse. The thin lines correspond to the quantum mechanical limit with the ratio $\lambda_{\mathrm{QM}} = \omega_z/\omega_r$ and the thick lines represent the Thomas-Fermi limit with the ratio $\lambda_{\mathrm{TF}} = (\omega_z/\omega_r)^2$. The crosses represent mixtures in the experiment which are found very close to the instability, whereas the dots indicate stable mixtures [27].

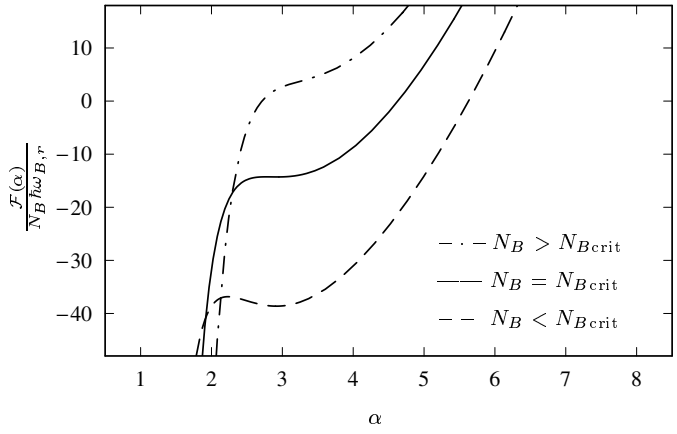

Fig. 6. Grand-canonical free energy $\mathcal{F}(\alpha)/N_B\hbar\omega_{B,r}$ versus the variational parameter α for various boson numbers N_B. A local minimum indicates a metastable state of the mixture.

free energy (29) and the negative last term describing the influence of the fermions. We have determined the stability border within the variational method in two different ways, which we discuss in the following sections.

4.3 Numerical integration

The most reliable approach is based on performing the integration in equation (29) numerically. We have evaluated the critical boson numbers $N_{B\mathrm{crit}}$ for different values of μ_F in an iterative way until the condition (51) is achieved with sufficient accuracy. The result is given by solid lines in the stability diagrams for the Hamburg and Florence experiment as shown in Figures 4 and 5, where the resulting particle number pairs (N_B, N_F) are smoothly connected with each other. The thick solid line of the Thomas-Fermi ratio $\lambda_{\mathrm{TF}} = (\omega_z/\omega_r)^2$ lies above, but near the dot-dashed line from the Gross-Pitaevskii equation in the Thomas-Fermi approximation in Section 4.1. This is expected as both the thick solid line and the dot-dashed line are evaluated in the Thomas-Fermi limit with the same ratio of the radial and axial extension of the BEC cloud. Furthermore, they show the same behavior for very large boson numbers as both lines become vertical so that the fermion number remains constant. In the Florence experiment both lines lie very close to the crosses of the experiment where the thick solid line fits them better. This is not surprising as the s-wave scattering length a_{BF} in Table 1 is determined with a mean-field analysis in the Florence experiment [27]. The thin solid line lies far below the thick solid line and reflects a mixture in the quantum-mechanical limit with the ratio $\lambda_{\mathrm{QM}} = \omega_z/\omega_r$. This line, which is a good approximation for mixtures with vanishing intraspecies and interspecies interactions, is less suitable for the ^{87}Rb–^{40}K mixture as the interaction energy is dominant according to Figure 2. Hence, the mixture can be well described in the Thomas-Fermi limit. As the thin solid line does not consider the proper ratio λ of the oscillator lengths in the test function (50) and, thus, minimizes the free energy less optimally for a strong interacting mixture, this line allows much smaller particle numbers in a stable mixture than the thick solid line. In order to estimate the ratio λ, which yields the stability border with the largest possible numbers for bosons and fermions, we have evaluated two lines in the stability diagram for ratios in the neighborhood of λ_{TF}, where one λ is 40% smaller and the other one is 40% larger. These lines for $\lambda = 0.6\lambda_{\mathrm{TF}}$ and $\lambda = 1.4\lambda_{\mathrm{TF}}$ are shown in Figure 7. Both lines lie throughout below, but very close to the original one with $\lambda = \lambda_{\mathrm{TF}}$. This indicates that the stability border in the Thomas-Fermi limit is stationary at $\lambda = \lambda_{\mathrm{TF}}$ where it possesses a maximum. Hence, the ratio λ_{TF} turns out to be the proper ratio for the ^{87}Rb–^{40}K mixture allowing the largest possible numbers for bosons and fermions in a stable mixture.

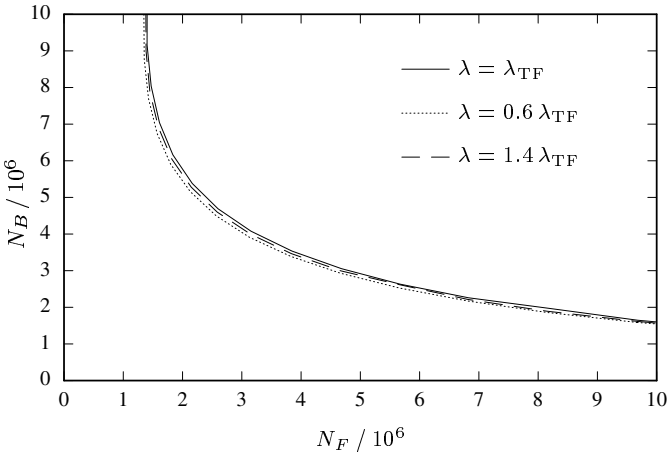

Fig. 7. Comparison of two stability borders whose ratio λ is 40% smaller and larger, respectively, than λ_{TF} in order to estimate the proper ratio λ which allows the largest possible particle number for a stable condensate of the Hamburg experiment.

4.4 Expansion with respect to interspecies interaction

Another approach was suggested in reference [24], where the local chemical potential (25) in the grand-canonical free energy (29) is expanded up to the third order in g_{BF} in order to get rid off the fractional power in the last term of the free energy. This expansion leads to Gaussian integrals with respect to the test function (50):

$$\mathcal{F}[\Psi_B^*,\Psi_B] = \int d^3x \Bigg[\frac{\hbar^2}{2m_B}|\boldsymbol{\nabla}\Psi_B(\mathbf{x})|^2 + V_{\mathrm{eff}}(\mathbf{x})|\Psi_B(\mathbf{x})|^2 + \frac{g_{\mathrm{eff}}}{2}|\Psi_B(\mathbf{x})|^4 + \frac{\kappa g_{BF}^3}{8\mu_F^{1/2}}|\Psi_B(\mathbf{x})|^6 + \ldots\Bigg], \quad (52)$$

where the terms with respect to the power of $|\Psi_B(\mathbf{x})|^2$ are summarized in the factors

$$V_{\mathrm{eff}}(\mathbf{x}) = \left[1 - \frac{3}{2}\kappa\mu_F^{1/2} g_{BF}\right]\frac{1}{2}m_B\omega_{B,r}^2(r^2+\lambda^2 z^2), \quad (53)$$

$$g_{\mathrm{eff}} = g_{BB} - \frac{3}{2}\kappa\mu_F^{1/2} g_{BF}^2. \quad (54)$$

Within this approximation it is assumed that the radius of the condensate is much less than the radius of the Fermi gas cloud so that the remaining expressions $(\mu_F - V_F(\mathbf{x}))^{n/2}$ with $n = 1, 3, 5$, arising from the expansion, can be expanded in powers of $V_F(\mathbf{x})/\mu_F$ as well. We consider therein only terms which depend on the parameter α. The last term in the free energy (52) corresponds to the elastic three-particle collision induced by the interspecies interaction. This term with $g_{BF} < 0$ is responsible for increasing both the bosonic and the fermionic particle density in the trap center in order to minimize the free energy. If the central condensate density $|\Psi_B(\mathbf{0})|^2$ becomes large enough due to large particle numbers, the positive first three terms in the free energy (52) cannot balance the negative last term in order to stabilize the mixture and to prevent it from collapsing. Performing the Gaussian integration in equation (52) leads to an algebraic equation with respect to the unknown quantities α and N_B:

$$\frac{\mathcal{F}(\alpha)}{N_B\hbar\omega_{B,r}} = \frac{2+\lambda}{4\alpha^2} + \frac{b(2+\lambda)\alpha^2}{3} + \frac{c_1 N_B}{\alpha^3} + \frac{c_2 N_B^2}{\alpha^6} + \ldots \quad (55)$$

with the factors

$$b = \frac{3}{4}\left[1 - \frac{3}{2}\kappa\mu_F^{1/2} g_{BF}\right],$$

$$c_1 = \frac{1}{2}\left[g_{BB} - \frac{3}{2}\kappa\mu_F^{1/2} g_{BF}^2\right]\frac{\lambda^{1/2}}{(2\pi)^{3/2}\hbar\omega_{B,r}L_{B,r}^3},$$

$$c_2 = \frac{\kappa\lambda g_{BF}^3}{3^{3/2}8\pi^3\hbar\omega_{B,r}\mu_F^{1/2}L_{B,r}^6}. \quad (56)$$

The condition (51) for the stability border provides two equations allowing to determine both unknown quantities for different values of μ_F. The result is shown in Figures 4 and 5 by the dashed line for both limits. The thick dashed as well as the thin dashed line converges with increasing fermion number N_F to the corresponding solid line of the numerical integration. But for low N_F or, equivalently large N_B, these dashed lines stay below the solid lines, where the discrepancy increases with decreasing N_F. Moreover, for very small N_F the dashed lines show the opposite behavior of the solid lines as they tend to zero, which seems to be unphysical. When the radius of the BEC clouds increases with decreasing N_F, the above mentioned expansion in powers of $V_F(\mathbf{x})/\mu_F$, which is done up to the zeroth and first order, fails as $V_F(\mathbf{x})$ and μ_F become comparable at the BEC cloud boundary. Thus, more orders of the expansion are needed to obtain more accurate results. Another reason is that the stability border in the stability diagram depends strongly on the interspecies s-wave scattering length a_{BF} according to the scaling law for the critical numbers of condensate atoms for a fixed ratio between N_B and N_F [27,41]:

$$N_{B\mathrm{crit}} \sim \frac{1}{a_{BF}^{12}}. \quad (57)$$

Thus, such a strong sensitivity of the critical boson number $N_{B\mathrm{crit}}$ with respect to a_{BF} and also to g_{BF} due to equation (7) does not justify an expansion of the local chemical potential $\tilde{\mu}_F(\mathbf{x})$ with respect to the smallness parameter g_{BF}.

4.5 Adjustment of a_{BF}

The above described strong dependence of $N_{B\mathrm{crit}}$ on a_{BF} allows us to extract a value for a_{BF} with great accuracy within a mean-field analysis of the stability as performed in this section. Because of the scaling law (57) the relative uncertainty of a_{BF} amounts to only a twelfth of the relative uncertainty of the critical boson number $N_{B\mathrm{crit}}$. As the thick solid line in Figure 5, which is based on the value

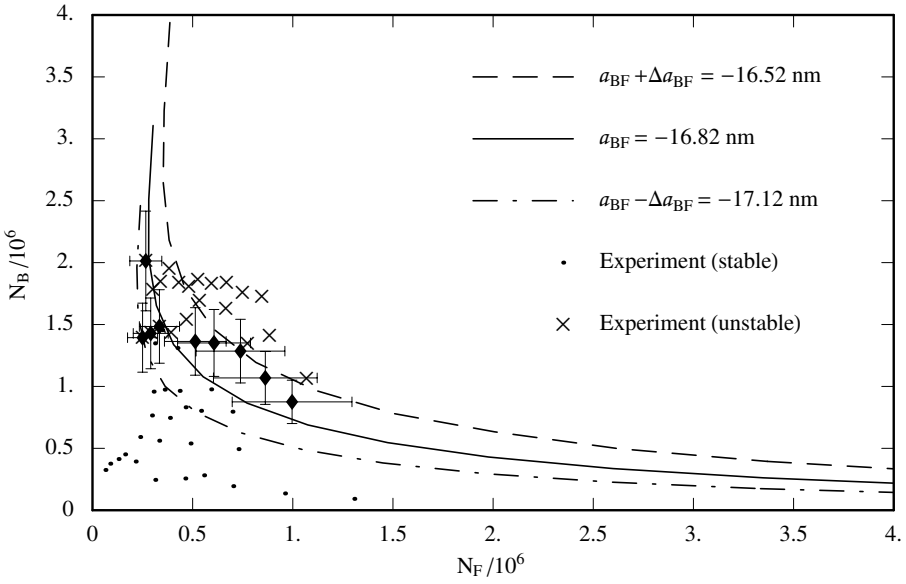

Fig. 8. Stability border for a new value $a_{BF} = (-16.82 \pm 0.30)$ nm of the ^{87}Rb–^{40}K mixture in the Hamburg experiment [6]. All three lines are obtained by numerical integrations of the fermionic density (35) according to Section 4.3 in the Thomas-Fermi limit with the ratio $\lambda_{\mathrm{TF}} = (\omega_z/\omega_r)^2$. Those stable (unstable) points, which are located above (below) the solid line, are equipped with error bars indicating a relative uncertainty of 20% and 30% for N_B and N_F, respectively, according to Figure 3 of reference [6].

$a_{BF} = -20.9$ nm for the Florence experiment [27], agrees quite well with the crosses of the experiments, we restrict ourselves here to fit a_{BF} to the data of the Hamburg experiment. In order to estimate the uncertainty of the latter, we have plotted in Figure 8 a dot-dashed (dashed) line comprising all crosses (dots) as a upper (lower) limit. The mean value for a_{BF} is chosen central between both limits and is represented by the solid line in Figure 8, which roughly separates the dots and the crosses. This estimation method is justified since those stable (unstable) points, which are located above (below) the solid line, extend with their total error $\Delta N = \sqrt{\Delta N_B^2 + \Delta N_F^2}$ over the solid line to the stable (unstable) sector. The new value $a_{BF} = (-16.82 \pm 030)$ nm differs only 12% from the old value $a_{BF} = -15.0$ nm, whereas the critical particle numbers between the dots and crosses are by a factor of around 3 smaller than those of the old thick solid line in Figure 4. Note that this new value for the interspecies s-wave scattering length leads also to a new value of the minimal fermionic particle number $N_{F,\min} = 1,95 \times 10^5$ below which the mixture is stable in accordance with the experimental data of Figure 8. Furthermore, we remark that the old value of a_{BF} was determined by the Sengstock group with the help of equation (55). However, instead of evaluating the respective fermion number N_F by integrating the fermionic density (35), they used the ad-hoc approximation [43]

$$\mu_F = \mu_F^{(0)} - \frac{g_{BF}}{g_{BB}}\mu_B^{(0)}, \tag{58}$$

where the noninteracting chemical potentials $\mu_B^{(0)}$ and $\mu_F^{(0)}$ are related to the respective particle numbers by equation (39). The above relation between disturbed and undisturbed chemical potentials is not correct.

5 Conclusion

Applying the Thomas-Fermi approximation in order to solve the Gross-Pitaevskii equation (17) for a stationary Bose-Fermi mixture in Section 3 reduces it from a differential to an algebraic equation (34). This allows to obtain an analytic expression for the bosonic and fermionic density profiles. The strong attraction between bosons and fermions gives rise to an increase of the particle densities within their overlap, accompanied by a shrinkage of the BEC and the Fermi gas cloud. In order to test the validity of the Thomas-Fermi approximation, we have plotted the kinetic energy of a boson together with its potential energy due to the trap, its intraspecies and its interspecies interaction energy, and the chemical potential as the total energy of a boson. This reveals the Thomas-Fermi approximation to be very good over a wide bulk range of the condensate cloud. The kinetic energy plays a significant role only in the outermost 10% of the BEC cloud.

Furthermore, we have found that the particle densities for both species become complex at sufficiently large particle numbers of bosons and fermions. We interpret this as a loss of the stability against collapse. The imaginary part of the density can be regarded as the decay rate of the described species and starts emerging in the trap center, where the densities have their maximum.

Beside the stability diagram arising from the complex solution of the Gross-Pitaevskii equation in the Thomas-Fermi approximation, we have evaluated the stability border within a variational method by extremizing the grand-canonical free energy (29) for a ^{87}Rb–^{40}K mixture with a Gaussian test function. The resulting lines for the variational method with a ratio of the oscillator lengths according to the Thomas-Fermi approximation show the same behavior as the ones of the Gross-Pitaevskii equation. Both lines are located close in the N_B-N_F-plane and

agree well. Finally, by comparing the calculated stability borders with the experimental values, we have found for the Florence experiment that the stability border of the variational method and of the Gross-Pitaevskii equation is in good agreement with the experimental results. For the Hamburg experiment, however, we have obtained a discrepancy between the calculated lines and the experimental results to which we have fitted the interspecies s-wave scattering length to $a_{BF} = (-16.82 \pm 0.30)$ nm. Despite this, there remains a discrepancy to the s-wave scattering length $a_{BF} = (-20.9 \pm 0.8)$ nm of the Florence experiment. As both experiments deal with a ^{87}Rb–^{40}K mixture, the interspecies s-wave scattering lengths should coincide. A possible explanation could be that the mean-field theory in this paper is developed for a stationary Bose-Fermi mixture and does not include dynamical aspects of the mixture. The dynamical behavior becomes important for a rapid cooling of the mixture which leads to a fast increase of the condensate density due to the occupation of all bosons into the ground state in a short time. We conclude with the remark that such dynamical effects within the Bose-Fermi mixture could be further investigated with the help of the coupled equations of motion (13) and (15).

We thank Kai Bongs, Konstantin Glaum, Aristeu Lima for critical comments as well as the DFG Priority Program SPP 1116 *Interactions in Ultra-Cold Atomic and Molecular Gases* for financial support.

References

1. A.G. Truscott, K.E. Strecker, W.I. McAlexander, G.B. Partridge, R.G. Hulet, Science **291**, 2570 (2001)
2. F. Schreck, L. Khaykovich, K.L. Corwin, G. Ferrari, T. Bourdel, J. Cubizolles, C. Salomon, Phys. Rev. Lett. **87**, 080403 (2001)
3. Z. Hadzibabic, C.A. Stan, K. Dieckmann, S. Gupta, M.W. Zwierlein, A. Görlitz, W. Ketterle, Phys. Rev. Lett. **88**, 160401 (2002)
4. G. Roati, F. Riboli, G. Modugno, M. Inguscio, Phys. Rev. Lett. **89**, 150403 (2002)
5. B. DeMarco, D.S. Jin, Science **285**, 1703 (1999)
6. C. Ospelkaus, S. Ospelkaus, K. Sengstock, K. Bongs, Phys. Rev. Lett. **96**, 020401 (2006)
7. N. Yokoshi, S. Kurihara, Phys. Rev. B **68**, 064501 (2003)
8. P. Capuzzi, E.S. Hernández, Phys. Rev. A **66**, 035602 (2002)
9. S. Ospelkaus, C. Ospelkaus, L. Humbert, K. Sengstock, K. Bongs, Phys. Rev. Lett. **97**, 120403 (2006)
10. G. Modugno, G. Roati, F. Riboli, F. Ferlaino, R.J. Brecha, M. Inguscio, Science **297**, 2240 (2002)
11. C.A. Regal, M. Greiner, D.S. Jin, Phys. Rev. Lett. **92**, 040403 (2004)
12. M.W. Zwierlein, A. Schirotzek, C.H. Schunck, W. Ketterle, Science **311**, 492 (2006)
13. L. Viverit, Phys. Rev. A **66**, 023605 (2002)
14. M.J. Bijlsma, B.A. Heringa, H.T.C. Stoof, Phys. Rev. A **61**, 053601 (2000)
15. M. Greiner, O. Mandel, T. Esslinger, Th.W. Hänsch, I. Bloch, Nature **415**, 39 (2002)
16. M. Lewenstein, L. Santos, M.A. Baranov, H. Fehrmann, Phys. Rev. Lett. **92**, 050401 (2004)
17. S. Ospelkaus, C. Ospelkaus, O. Wille, M. Succo, P. Ernst, K. Sengstock, K. Bongs, Phys. Rev. Lett. **96**, 180403 (2006)
18. K. Günter, T. Stöferle, H. Moritz, M. Köhl, T. Esslinger, Phys. Rev. Lett. **96**, 180402 (2006)
19. N. Nygaard, K. Molmer, Phys. Rev. A **59**, 2974 (1999)
20. R. Roth, H. Feldmeier, Phys. Rev. A **65**, 021603 (2002)
21. R. Roth, Phys. Rev. A **66**, 013614 (2002)
22. T. Miyakawa, T. Suzuki, H. Yabu, Phys. Rev. A **64**, 033611 (2001)
23. S.T. Chui, V.N. Ryzhov, Phys. Rev. A **69**, 043607 (2004)
24. S.T. Chui, V.N. Ryzhov, E.E. Tareyeva, JETP Lett. **80**, 274 (2004)
25. S.K. Adhikari, Phys. Rev. A **70**, 043617 (2004)
26. X. Liu, M. Modugno, H. Hu, Phys. Rev. A **68**, 053605 (2003)
27. M. Modugno, F. Ferlaino, F. Riboli, G. Roati, G. Modugno, M. Inguscio, Phys. Rev. A **68**, 043626 (2003)
28. G. Ferrari, M. Inguscio, W. Jastrzebski, G. Modugno, G. Roati, A. Simoni, Phys. Rev. Lett. **89**, 053202 (2002)
29. S. Inouye, J. Goldwin, M.L. Olsen, C. Ticknor, J.L. Bohn, D.S. Jin, Phys. Rev. Lett. **93**, 183201 (2004)
30. J. Goldwin, S. Inouye, M.L. Olsen, B. Newman, B.D. DePaola, D.S. Jin, Phys. Rev. A **70**, 021601(R) (2004)
31. F. Ferlaino, C. D'Errico, G. Roati, M. Zaccanti, M. Inguscio, G. Modugno, A. Simoni, Phys. Rev. A **73**, 040702(R) (2006); F. Ferlaino, C. D'Errico, G. Roati, M. Zaccanti, M. Inguscio, G. Modugno, A. Simoni, Phys. Rev. A **74**, 039903(E) (2006)
32. W. Greiner, J. Reinhardt, *Field Quantization*, 1st edn. (Springer, Berlin, 1996)
33. H. Kleinert, *Path Integrals in Quantum Mechanics, Statistics, Polymer Physics, and Financial Markets*, 4th edn. (World Scientific, Singapore, 2006)
34. C.J. Pethick, H. Smith, *Bose-Einstein Condensation in Dilute Gases* (Cambridge University Press, Cambridge, 2002)
35. F. Dalfovo, S. Giorgini, L.P. Pitaevskii, S. Stringari, Rev. Mod. Phys. **71**, 463 (1999)
36. B. De Witt, *Dynamical Theory of Groups and Fields* (Gordon and Breach, New York, 1965)
37. R. Jackiw, Phys. Rev. D **9**, 1686 (1974)
38. L.P. Pitaevskii, Zh. Eksp. Teor. Fiz. **40**, 646 (1961) [Sov. Phys. JETP **13**, 451 (1961)]
39. E.P. Gross, Nuovo Cimento **20**, 454 (1961)
40. N.W. Ashcroft, N.D. Mermin, *Solide State Physics*, International edn. (Saunders College, Philadelphia, 1976)
41. K. Molmer, Phys. Rev. Lett. **80**, 1804 (1998)
42. W. Greiner, *Classical Mechanics: Systems of Particles and Hamiltonian Dynamics*, 1st edn. (Springer, Berlin, 2002)
43. J.M. Goldwin, Ph.D. thesis, University of Colorado (2005)